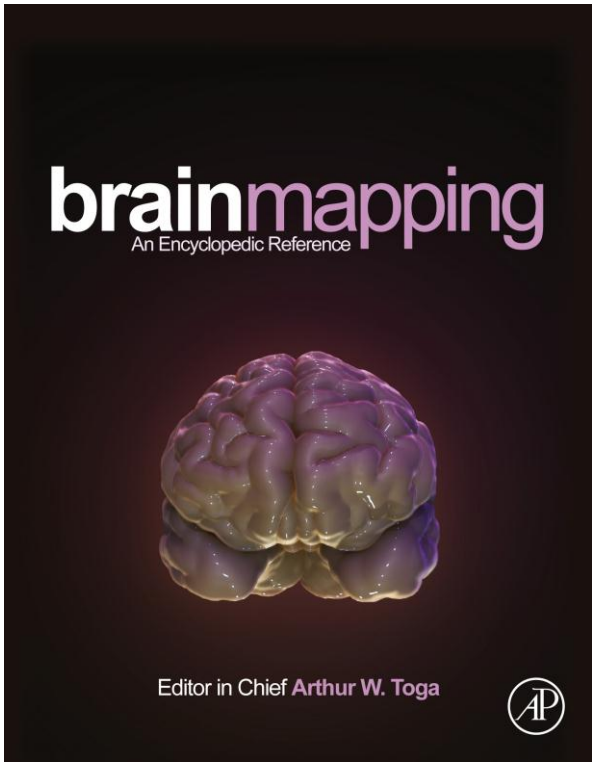

Vogt B.A. (2015) Mapping Cingulate Subregions. In: Arthur W. Toga, editor. *Brain Mapping: An Encyclopedic Reference*, vol. 2, pp. 325-339. Academic Press: Elsevier.

Mapping Cingulate Subregions

BA Vogt, Cingulum NeuroSciences Institute, Manlius, NY, USA; Institute of Neuroscience and Medicine (INM-1), Jülich, Germany; Boston University School of Medicine, Boston, MA, USA

Glossary

CML Caudomedial lobule of vPCC.
Dysgranular Variable thickness layer IV where layer IIIc and Va pyramids may abut.
ECG External cingulate gyrus formed by area 32.
Granular A well-defined layer IV.
NeuN Neuron-specific nuclear binding protein; antibody for neurons without coreacting with glial or vascular elements.
Perisplenial A general area around the splenium of the corpus callosum.
SMI32 Antibody to intermediate neurofilament proteins.

Abbreviations

aMCC Anterior midcingulate cortex
CG Cingulate gyrus
cgs Cingulate sulcus
dPCC Dorsal posterior cingulate cortex
pACC Perigenual anterior cingulate cortex
pMCC Posterior midcingulate cortex
RSC Retrosplenial cortex; areas 29 and 30.
sACC Subgenual anterior cingulate cortex
Spls Splenial sulci
vPCC Ventral posterior cingulate cortex

Nomenclature

′ The prime designates areas in midcingulate cortex

Vogt and Vogt (1919) published the most thorough map of areas on the human medial surface. There was, however, little histological documentation of the area features, and it has yet to be fully appreciated. Figure 1 shows this masterpiece and points to many correlations with current findings: The red asterisks emphasize nine divisions of area 32 and the numbers (with arrows) refer to the following:

(1) There are two vertical and one horizontally oriented division of area 25.
(2) There are four longitudinally oriented areas (starting at the corpus callosum) we refer to as areas 33, 24a, 24b, and 24c.
(3) There is a significant vertical border above the rostrum of the corpus callosum, which is the border between the anterior cingulate cortex (ACC) and the midcingulate cortex (MCC).
(4) There are four subdivisions of the anterior MCC (a33′, a24a′, a24b′, and a24c′), and the parenthesis emphasizes the posterior MCC and its divisions.
(5) There is a continuation of motor cortex that emerges on the medial surface (primitive gigantopyramidal field, Braak, 1976; and area 24d, Luppino, Matelli, Camarda, Gallese, & Rizzolatti, 1991). The marginal ramus (mr) of the cingulate sulcus (cgs) was opened for their area 75 (part of area 23c).
(6) Area 23d forms the rostral, dysgranular part of dorsal posterior cingulate cortex (dPCC).
(7) Divisions of dPCC including areas d23a and d23b.
(8) The retrosplenial areas on the ventral bank of the cingulate gyrus (CG).
(9) Ventral PCC.
(10) The ventral area 31 caudal to area 23.

Thus, the essential organization of cingulate cortex was known by the Vogt's early in the twentieth century, and although human functional imaging has yet to resolve these elegant observations, this remains the challenge for the coming decades.

Obviously, Brodmann's (1909) map reflected broad strokes rather than precise histology. Whereas Brodmann identified four areas in ACC (areas 25, 33, 32, and 24), the Vogt's identified 41 areas and our current map designates 21 areas. The cytoarchitecture is so different in parts of Brodmann's areas 24 and 32 that they cannot be considered the same area or even part of the same region. Importantly, no investigator has ever activated Brodmann's entire ACC in a functional imaging study meaning that it does not have a single underlying function, and the importance of this fact has yet to be fully appreciated; Brodmann's ACC is not a structure/function region.

Beyond cytoarchitectural differentiations of ACC and MCC (see the succeeding text), ligand binding autoradiography is a valuable adjunct to cytoarchitectural studies (Palomero-Gallagher, Mohlberg, Zilles, & Vogt, 2008; Palomero-Gallagher, Schleicher, Zilles, & Vogt, 2013; Palomero-Gallagher, Vogt, Mayberg, Schleicher, & Zilles, 2009) and provides an elegant demonstration that Brodmann's ACC is not uniform.

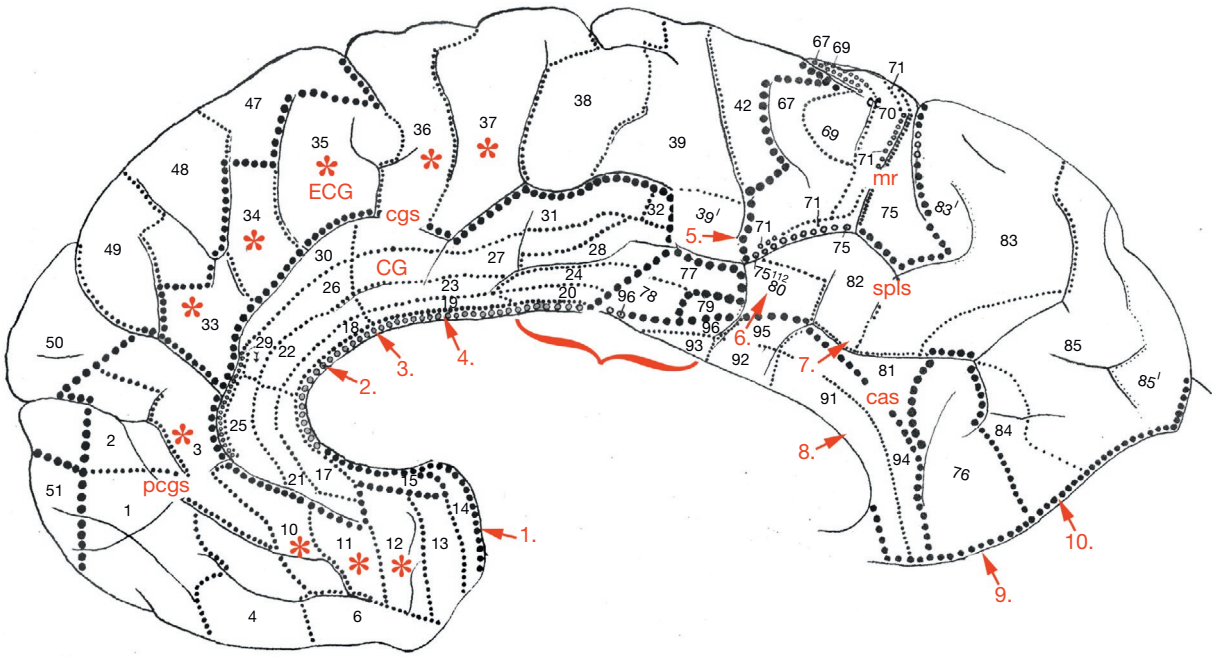

Figure 1 Vogt and Vogt's (1919) map of areas on the medial surface (two images in their Figure 51 merged). The red highlights were added as an aid to interpreting this work in the context of recent findings. The most important are the horizontal divisions within the cingulate gyrus (2), the border between ACC and MCC (3), the nine divisions of area 32 (asterisks), the two parts of MCC (4), the border between aMCC and pMCC (parenthesis marking pMCC), and an extension of motor cortex into the cingulate sulcus (5). cas, callosal sulcus; CG, cingulate gyrus; cgs, cingulate sulcus; ECG, external cingulate gyrus; mr, marginal ramus of the cgs; spls, splenial sulci.

Figure 2 shows his ACC divided into anterior and posterior parts (at pointer) (arrows show coronal section positions). Sections in Figure 2(b) are autoradiographs for two of the 15 receptors that were chosen because an 'asymmetry index' showed them to be statistically different (Palomero-Gallagher et al., 2009). Clearly, $GABA_A$ receptors are quite low in anterior area 24, while they are extremely high in layers I–III of posterior area 24. In contrast, α-amino-3-hydroxy-5-methyl-4 isoxazole-proprionic acid receptors are very high in layers I–V in anterior area 24 but extremely low in posterior area 24. A polar plot of 15 receptors (Figure 2(c)) is of binding throughout the entire area, and receptors that are significantly different in each subregion are noted with asterisks. Eight of the 15 neurotransmitter receptors differed significantly in the two divisions. Thus, the anterior and posterior parts of Brodmann's ACC are qualitatively different in their neurochemistry and connections.

Although the midcingulate concept arose from a cytoarchitectural study (Vogt Nimchinsky, Vogt, & Hof, 1995), this and other neurobiological differences have emerged including functional imaging (Palomero-Gallagher et al., 2008, 2009; Vogt, 2009a, 2009b; Vogt & Palomero-Gallagher, 2012; Vogt, Vogt, & Laureys, 2006; Yu et al., 2011) to support the hypothesis that MCC differs qualitatively from ACC. Thus, MCC is *not* a division of ACC, and studies that subdivide ACC into dorsal, rostral, ventral, or caudal are employing Brodmann's century-old view without reference to substantial recent observations. They also overlook the predictive nature of the eight-subregion model. Following on this issue, it is often said that the name for a subregion is simply a matter of consensus. Ernst Mach stated, "to name is to classify, to establish ideal affiliations – analogous relationships – between little known phenomena, and to identify the general idea or principle wherein they lie latent" (Cajal, 1999). In fact, MCC represents more than a name; it represents a fundamentally different model of cingulate organization based on numerous neurobiological observations that reflect the general principle wherein the fundamental organization of cingulate cortex lies latent. Since this new model cannot be verified with a single imaging method, it is a conceptual perspective based on cytoarchitecture, receptor binding, and functional studies.

Finally, the first principle of neuroanatomy is that every major structural difference predicts an important functional difference. Embedded in every cytoarchitectural study is the fact that projections arise from neurons of different sizes in each layer. For example, we identified the structural differences between ACC and MCC (Vogt et al., 1995). Bush, Luu, and Posner (2000) later performed a meta-analysis of the affective and cognitive divisions, and this border matched the cytoarchitectural border (Figure 3(a)). Areas and layers will ultimately be the foci of functional studies; however, this will require higher-resolution imaging. Although we are now transitioning from the regional to the subregional level of analysis, future studies will resolve individual areal and laminar functions. Thus, the cytology of areas and layers must be considered, particularly because networks are composed of neurons in particular layers and future network models will be devised around neuronal architecture rather than area activity.

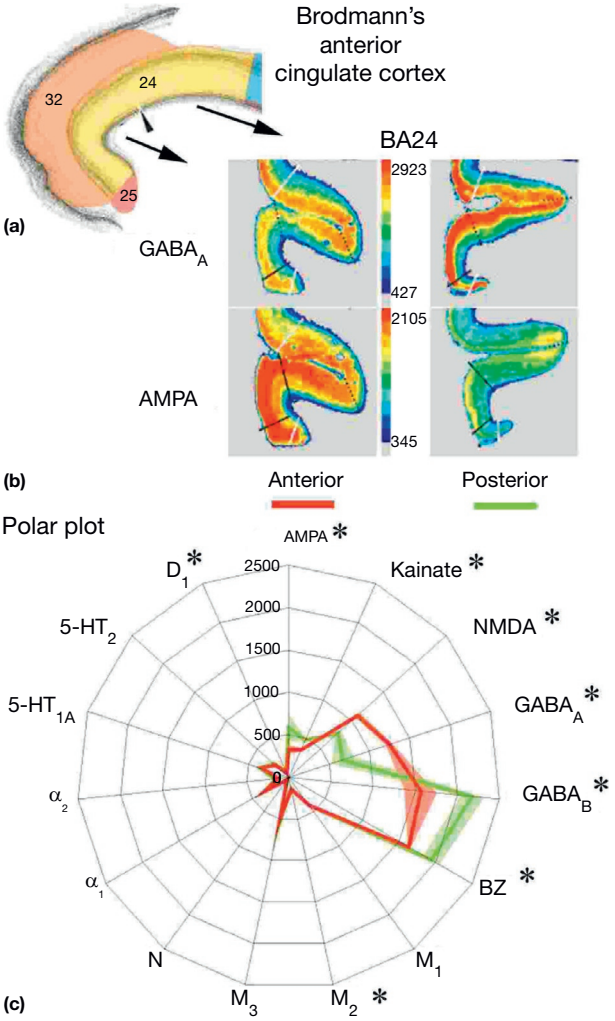

Figure 2 Assessment of 15 neurotransmitter receptors in the anterior and posterior parts of Brodmann's area 24. (a) Map of his anterior cingulate region with a pointer separating its two parts used in the analysis. (b) Coronal sections for two receptors through each part show a radical difference in the laminar patterns of binding. (c) Polar plots for anterior (red line ± SD) and posterior (green line ± SD) with asterisks emphasizing the receptors that are statistically significant. The null hypothesis was rejected, and these findings validate the midcingulate concept; that is, caudal ACC is not a part of ACC. Modified from Palomero-Gallagher et al. (2009) Receptor architecture of human cingulate cortex: insights into the four-region neurobiological model. *Human Brain Mapping* 30: 2336–2355.

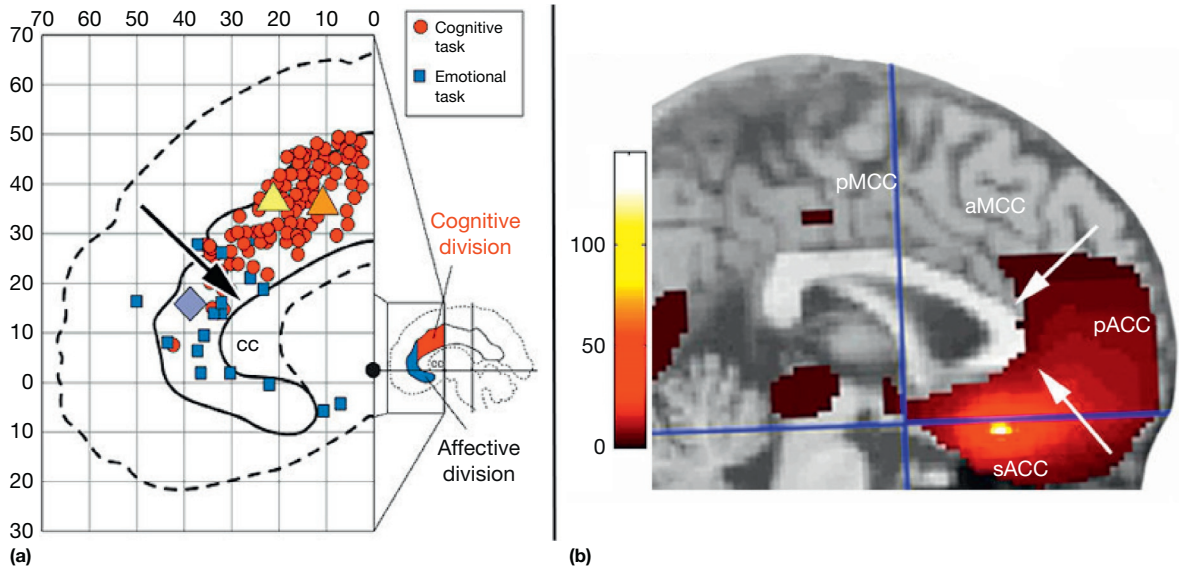

Figure 3 (a) Meta-analysis of Bush et al. (2000) showing activity in the affective and cognitive divisions of cingulate cortex. The black arrow marks the border between pACC and aMCC. (b) Correlations of resting glucose metabolism seeded in area s32 showing the functional independence and border between ACC and MCC.

Subregional Cytoarchitecture

Cingulate Flat Map

A complete flat map of cingulate areas (Vogt, 2009b) is in Figure 4(a). The Talairach and Tournoux (1988) coordinate system is overlayed on the map, and overlaying these two systems is an approximation as the latter coordinates are for a brain that is not characteristic of most, individual areas have a high degree of variability, and their landmarks and proportional grid system are inconsistent (Amunts, Malikovic, Mohlberg, Schormann, & Zilles, 2000; Grachev et al., 1999; Li, Freeman, Tran-Dinh, & Morris, 2003; Nowinski, 2001). Our flat map was derived from a healthy control GPC who was an 80-year-old, right-handed, white male who died from pneumonia and retroperitoneal hemorrhage. There was no evidence of neurological or psychiatric disorders, and the brain had an unremarkable postmortem histology. The left hemisphere is used throughout this article but is flipped for coregistration to some findings.

Flat map construction begins with histological sections (Figure 4(b)) onto which the midcortical layer is drawn. The apices and fundi of each gyrus and sulcus, respectively, are marked and the distances between each pair determined (Figure 4(c)). These lines are flattened (Figure 4(d)) and their intersection distance retained along the corpus callosum. The sulci are opened rostral and caudal to the corpus callosum (double arrows; Figure 4(a)). The largest sulci have been exposed and filled with a uniform gray to show sulcal areas: paracingulate sulcus (pcgs), cgs, splenial sulci (spls), and callosal sulcus (cas). The splenium was rotated ventrally at the small dotted line to expose the retrosplenial cortex (RSC), and the length of the corpus callosum is shown with a red double arrow. The external cingulate gyrus (ECG) and CG are also noted. Since this is a flat map, the Talairach and Tournoux

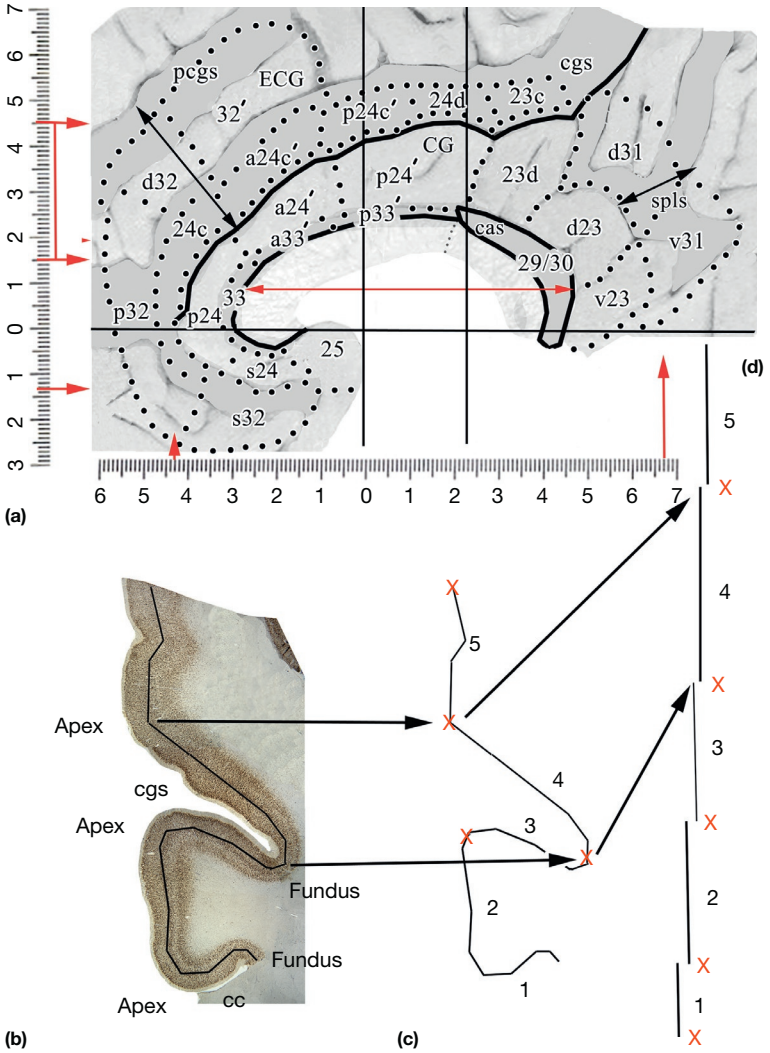

Figure 4 (a) Flat map of cingulate areas with the coordinates from Talairach and Tournoux (1988). The flattening orientations are shown with double arrows over the genu and behind the splenium of the corpus callosum. As the splenium was rotated ventrally to expose the ventral bank of the cgs to show areas 29 and 30, the actual length of the corpus callosum is shown with the red double arrow. (b) A histological section with the midcortical layer marked. (c) The latter line is broken into segments and measured. (d) The segments are flattened and used to derive the flat map.

coordinates are not accurate for all of the cingulate cortex, and red arrows on the coordinate scales alert to where they are useful and where they are not due to opening of the sulci. They are useful in the *y*-axis at +4.3 to −6.7 cm and in the *z*-axis between −1.3 and +1.5. Since the cgs is maintained intact but is exposed and extended dorsally, *z*-axis coordinates between +1.5 and +4.5 are only accurate for the CG surface. Activation sites are coregistered to this map using the dorsal apex of the corpus callosum and cgs as landmarks.

Subgenual and Perigenual ACC

James (1884) proposed that emotion is dependent on peripheral autonomic feedback. This association is made in ACC, which stores emotional (valenced) memories of objects and events and has autonomic afferent and regulatory functions. The subgenual ACC (sACC) projects to visceral regulatory nuclei including the central nucleus of the amygdala, parabrachial nucleus, and lateral hypothalamus (review Vogt & Vogt, 2009). Bancaud and Talairach (1992) made a critical distinction between ACC and MCC; the most frequent response to medial cortex electrical stimulation was intense or overwhelming fear including one individual who reported the feeling that death was imminent. Stimulation of ACC evoked the report, "I was afraid and my heart started to beat," whereas stimulation of MCC evoked the report, "I felt something, as though I was going to leave." The former report is one of pure fear, while the latter is early premotor planning with motivational features. Electrical stimulation of areas 25 and 24 evokes changes in respiratory and cardiac rates and blood pressure, mydriasis, piloerection, and facial flushing (Escobedo, Fernández-Guardiola, & Solis, 1973; Pool, 1954) and gastrointestinal responses included nausea, vomiting, epigastric sensation, salivation, or bowel or bladder evacuation (Meyer, McElhaney, Martin, & McGraw, 1973; Pool & Ransohoff, 1949). Also, blood flow is elevated in sACC when healthy women recall sad experiences (George et al., 1995; Mayberg et al., 1999) and when subjects evaluate emotional faces (George et al., 1993).

Cingulate gyral surface cytoarchitecture in ACC and MCC is shown in **Figure 5** with pairs of sections for neuron-specific nuclear binding protein (NeuN antibody) and intermediate neurofilament proteins (SMI32 antibody). The sACC is composed of areas 25, s33, s24, and s32, while the perigenual ACC (pACC) includes areas p33, p24a–c, and p32 (Palomero-Gallagher et al., 2008). **Figure 5(e)** shows that area 25 has a rudimentary architecture with external (layers II–III) and internal (V–VI) pyramidal layers that have little differentiation, while areas 24 and 32 have differentiated layers III and Va and a dysgranular layer IV in the latter. The lack of layer V differentiation in area 25 is particularly notable with the SMI32 section, since neurofilament proteins are expressed by large projection neurons.

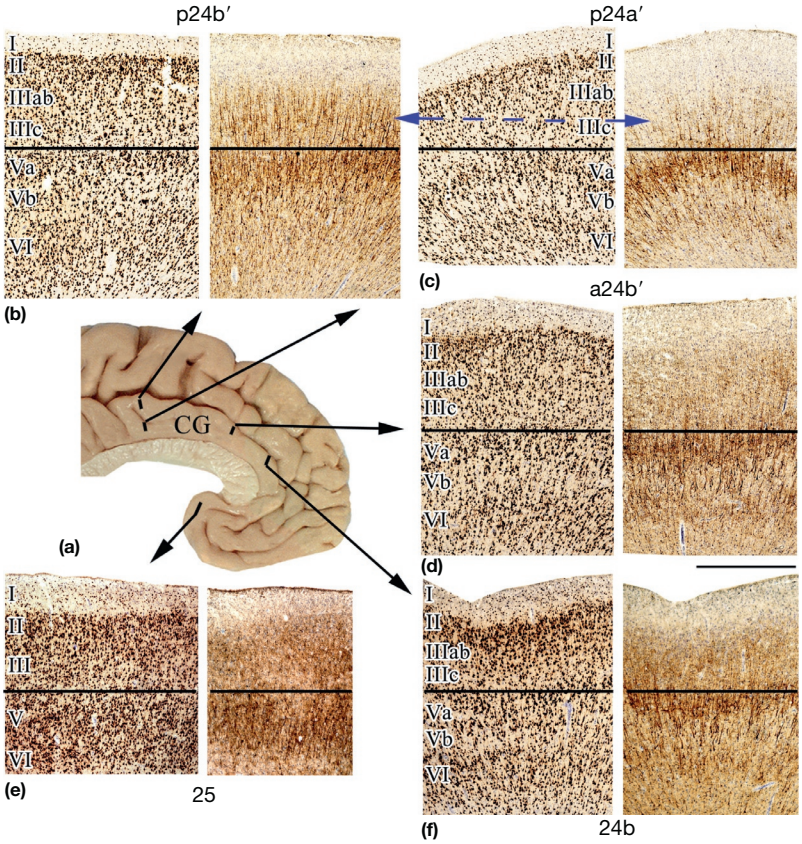

Figure 5 Cytoarchitecture of the gyral surface in ACC and MCC including sampling sites for pairs of NeuN and SMI32 images (a). The blue dashed arrow emphasizes the substantial expression of intermediate neurofilament proteins in layer III of area p24b′ compared with those in area p24a′. Scale bar, 1 mm.

Laminar differentiation is shown in Figure 5 from ventral to caudal cingulate areas. Area 24b layer III (Figure 5(f)) is differentiated from layer II, although layer II is quite broad and layers Va–VI are more apparent than in area 25. Layer III in area 24b has some large pyramids expressing neurofilament proteins, although they are fewer than in area 25. The number of these latter neurons is greatly reduced in layer III of areas a24b′ and p24b′, while in area p24b′, they emerge again as the trend to very large pyramids in layer IIIc asserts itself throughout PCC.

There are four divisions of area 32 (Palomero-Gallagher et al., 2008) with cytoarchitecture and ligand binding differences (Figure 6). The key cytoarchitectural difference occurs in layer III where there is a progressive shift in the largest pyramids in layer IIIab in area s32 to the deep part of layer IIIc in area 32′. There is also a progressive reduction in neuron densities in layers Va and Vb. The fingerprints of ligand binding for the mean of all layers (Figure 6(b)) and the laminar binding patterns for benzodiazepine (BZ) (Figure 6(c)) and $GABA_B$ (Figure 6(d)) receptors are shown. The BZ binding is most dense in layers III–IV of area s32, and it is progressively lower in areas p32, d32, and 32′. Although a similar trend occurs for $GABA_B$ binding, that for area d32 is higher than that for area p32.

Anterior and Posterior MCC

Brodmann (1909) realized the need for a structure between ACC and RSC in rodents where he placed 'area 23'; however, he recognized that it did not have a layer IV as in primates. In fact,

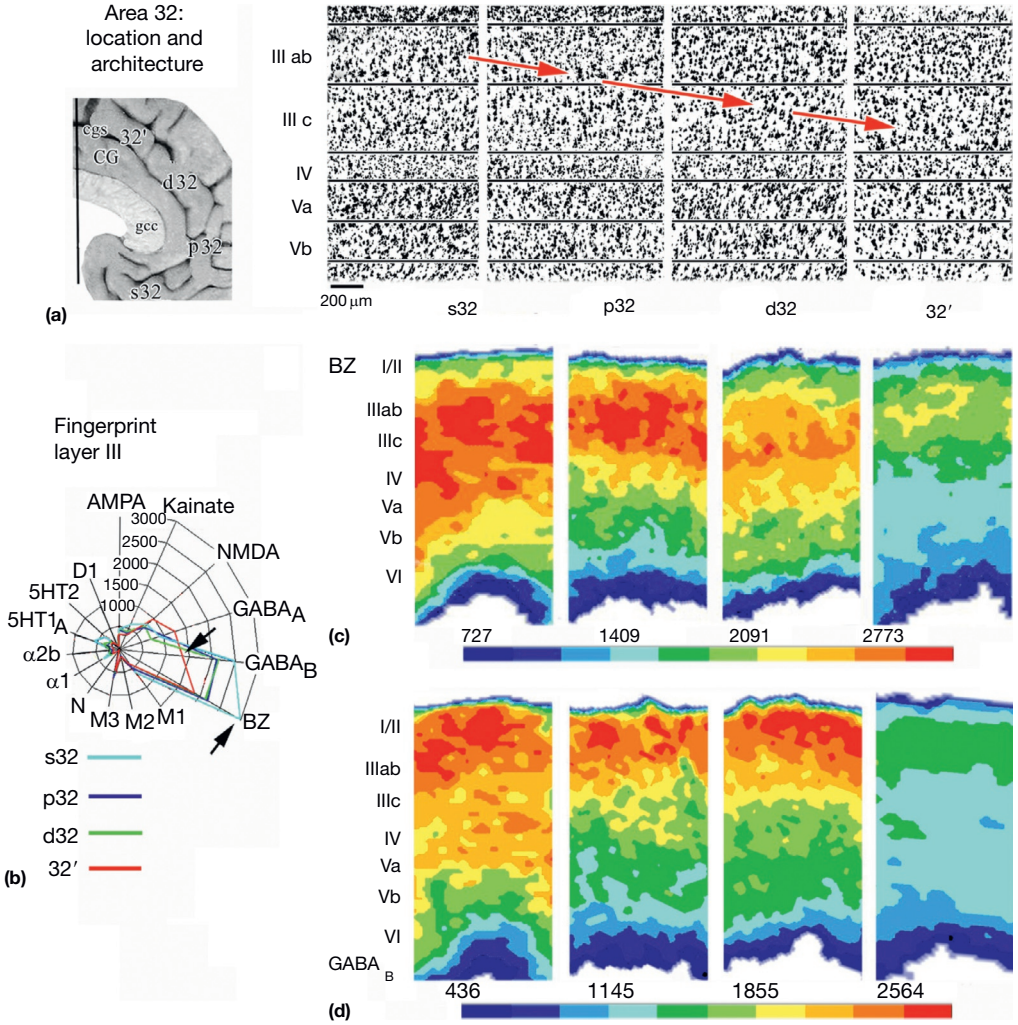

Figure 6 (a) Location of each sample site and associated cytoarchitecture of four divisions of area 32. The red arrows draw attention to the progressive shift in the largest neurons in layer IIIab of area s32 to layer IIIc in area 32′. (b) Fingerprint of binding for 15 receptors in layer III with arrows emphasizing significant differences in $GABA_B$ and benzodiazepine (BZ) binding. (c) Laminar profiles in binding showing the highest BZ mainly in layers III and IV and progressive reduction in binding from area s32 to area 32′. $GABA_B$ binding is more concentrated in layers II and IIIab and undergoes significant changes with area s32 having the broadest distribution of receptors and area 32′ the fewest. The laminar differences in binding confirm cytoarchitectural findings of four divisions of area 32. Reproduced from Vogt, B. A., & Palomero-Gallagher, N. (2012). Cingulate cortex. In: G. Paxinos & J. K. Mai (Eds.), *The human nervous system* (3rd ed.). (pp. 943–987). Academic Press, Chapter 25.

this is MCC in rodents (Vogt & Paxinos, 2014). Thus, along with the Vogt and Vogt's (1919) map of areas on the medial surface (**Figure 1**), MCC was already emerging at the beginning of the twentieth century. One strategy for identifying the ACC/MCC border is with correlations among clusters of voxels in basal glucose metabolism, and **Figure 3(b)** shows a statistical parametric map for 153 healthy subjects. The correlation was seeded in area s32 and correlated clusters were identified (Vogt, 2009a). The entire ACC has significant correlations with area s32 and suggests that the histological ACC operates as a metabolic unit rather than the broader anterior cingulate construct of Brodmann. Also, ACC and MCC have significantly different levels of basal glucose metabolism and support their independent functionality.

The MCC is composed of anterior and posterior divisions (aMCC and pMCC) (Vogt Berger, & Derbyshire, 2003). The two premotor areas in the cgs have large layer Vb neurons in aMCC and pMCC with unique cytoarchitectures, and the gyral surface shows differences that parallel those in the sulcus. For example, areas a24b′ (**Figure 5(d)**) and p24b′ (**Figure 5(b)**) distinguish aMCC and pMCC. Although layer III appears similar in both areas with NeuN, the latter has robust expression of neurofilament proteins by large layer III pyramids, there is a substantial increase in the breadth of layers V and VI, and layer VI neurons are smaller than in the former area.

A very important study by Enriquez-Geppert et al. (2013) functionally differentiated aMCC and pMCC. They showed that conflict manipulated by congruency of flanking stimuli relative to a target (congruent vs. incongruent) and motor inhibition by a within-trial response change of the initiated response (keep response vs. stop-change) was associated with two principal components: High conflict on incongruent trials activated pMCC (PC1) and stop-change trials modulated aMCC (PC2). This is a critical validation of the dichotomy of MCC structure and function and provides tests for patients that have a selective impairment in one of these two subregions, for example, disruption of glucose metabolism in pMCC in posttraumatic stress disorder (Shin et al., 2009).

Cingulate Premotor Areas

Electrical stimulation of MCC evokes complex and context-dependent gestures such as touching, kneading, rubbing or pressing the fingers or hands together, and lip puckering or sucking (Meyer et al., 1973; Talairach et al., 1973). These movements are often adapted to the environment and can be modified by sensory stimuli and resisted. The concept of 'attention-for-action' proposed by Posner, Peterson, Fox, and Raichle (1988) provided an early premotor orientation for MCC function. These areas contain neurons with premotor discharge properties (Shima et al., 1991) coded according to the changing reward properties of particular behaviors (Shima & Tanji, 1998), and human imaging shows altered blood flow during sequences of complex finger apposition movements (Kwan, Crawley, Mikulis, & Davis, 2000).

Braak (1976) played a critical role in introducing the modern era of cingulate neurobiology when he reported the primitive gigantopyramidal field in the caudal cgs with pigment architecture. This field was subsequently termed area 24d in monkeys by Luppino et al. (1991). **Figure 7(e)** and **7(f)** shows the key features of this area including a pigment architecture preparation kindly provided by Heiko Braak (**Figure 7(f)** PA). Spinal projections were first shown by Biber, Kneisley, and LaVail (1978) and Nudo and Masterton (1990), and area 24d has a neuron dense layer Va and sparse layer Vb, the latter of which contains large corticospinal projection neurons visible with NeuN and SMI32.

Figure 7 also shows area p24c′ in comparison with area 24d and gyral surface areas p24a′ and p24b′. Area p24c′ has very dense and broad layers Va and Vb compared with all areas at this level. As is the case for area a24′, p24b′ has a broader layer IIIc than p24a′ with pyramids that are larger and express substantially more neurofilament proteins. Large neurons in layer Vb of area p24b′ are smaller than those in p24c′ (red asterisks; **Figure 7(d)**).

The border between the two premotor cortices is rostral to the vertical plane at the anterior commissure, and this cortex is composed of five areas: areas 24c and a24c′ form the rostral cingulate premotor area and areas p24c′, 24d, and 23c form the caudal cingulate premotor area. These are premotor rather than motor areas for a number of reasons: (1) Although they have spinal projections, compared to motor and supplementary motor cortices, the projections are only about one-quarter as dense; (2) they are involved in more than motor functions including anticipation of performing a task long before an overt action and other cognitive functions (Kirsch et al., 2003; Murtha, Chertkow, Beauregard, Dixon, & Evans, 1996); and (3) area 24c′ has a particularly high level of dopamine-1 receptors (**Figure 8**) suggesting that it has a role beyond motor function such as coding the reward value of stimuli and contexts.

Palomero-Gallagher and Zilles (2009) published a thorough assessment of the cingulate subregional, areal, and laminar distributions of binding for 15 neurotransmitter receptors. **Figure 8** provides sulcal binding for four ligands derived from this work and NeuN for comparison. The cytology shows that layer Vb in all of the premotor areas has some large pyramids as predicted from the distribution of corticospinal projection neurons. The largest, however, are in areas a24c′, p24c′ (not shown), and 24d. The following observations are of particular note: (1) Kainate receptors are most dense in layers V and VI, while AMPA and NMDA receptors are mainly in layers I–III/IV in area 23c. The corticospinal neurons themselves are likely under heavy regulation by kainate receptors, although their apical dendrites in the superficial layers participate in other glutamatergic functions. (2) Kainate receptors undergo a progressive diminution in density from rostral to caudal premotor areas. (3) NMDA receptor densities are approximately equivalent as are $GABA_A$ receptor densities except for area 24d. This is a common feature, therefore, for all of the premotor areas. The fact that area 24d is under weak inhibitory control may have significant functional consequences. (4) Area 24c′ has the highest density of dopamine-1 receptors suggesting its involvement in coding the reward value of stimuli and contexts. Thus, the cingulate premotor areas share many similarities in terms of neuron composition and transmitter receptor binding. Finally, area 23c is unique as it has a layer IV and relatively the highest superficial layer $GABA_A$ regulation and the lowest density of deep-layer kainate receptors.

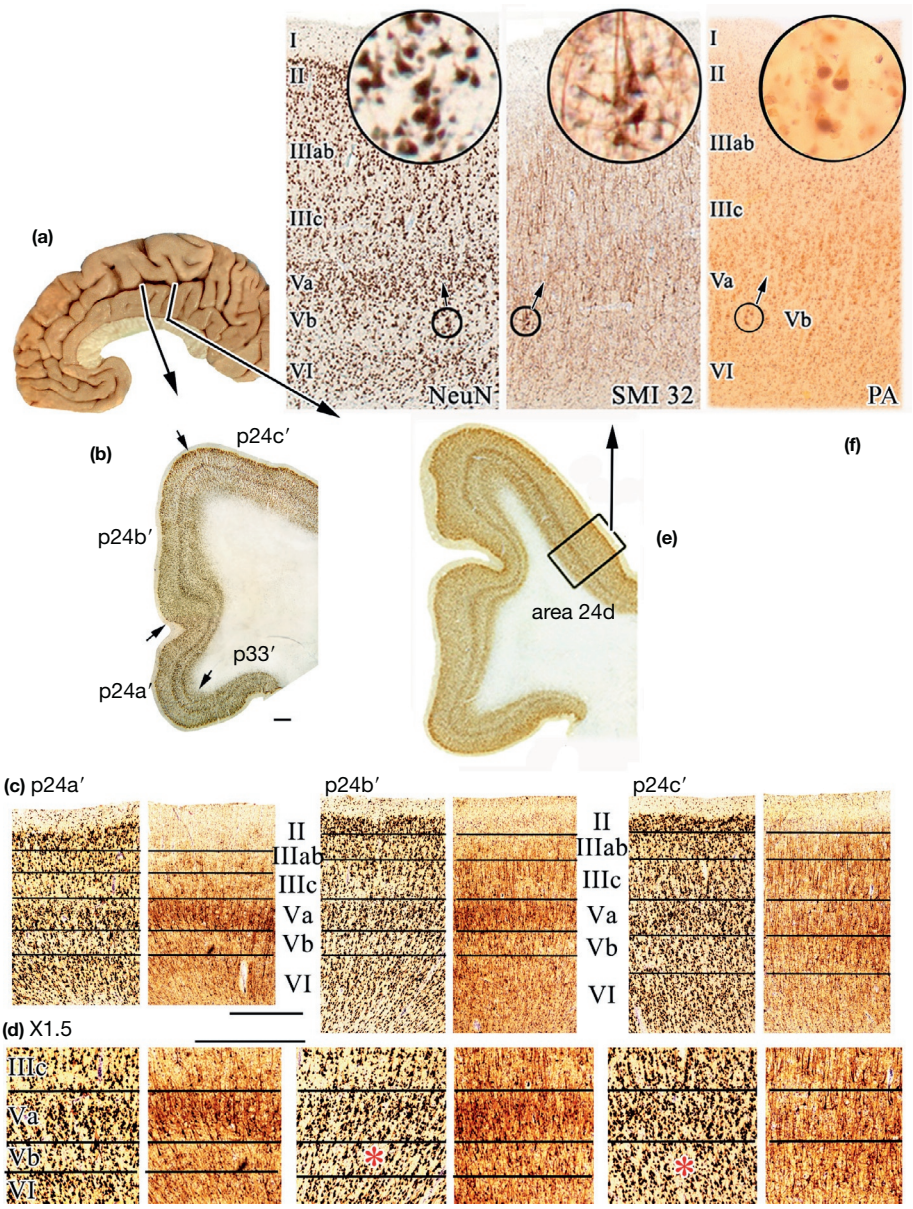

Figure 7 The cingulate premotor areas and adjacent areas on the gyral surface. (a) Sampling sites (different orientations due to a change in the plane of section). (b) Section through area p24′. (c) Higher magnification of three p24′ areas and (d) magnification of sections in (c) by 1.5×. The red asterisks in layer Vb emphasize the largest neurons in area p24c′ compared with those in area p24b′. (e) Section through area 24d. (f) Three preparations of area 24d including pigment architecture (PA) originally used by Heiko Braak to identify this area. These three photographs provide a means of extrapolating from the PA to NeuN and SMI32 preparations. Scale bar, 100 μm.

Dorsal and Ventral Posterior Cingulate Cortex

Dorsal PCC (dPCC) is involved in topographic and topokinetic memory, that is, orientation of the body in space. Olson, Musil, and Goldberg (1993, 1996) proposed that it is involved in large visual scene assessment, part of which is subserved by the orbital position of the eye and that the orbital position signal is used to generate a map of the head and body in space. Mental navigation along memorized routes elevates blood flow in PCC (Berthoz, 1997; Ghaem et al., 1997; Maguire, Frith, Burgiss, Donnett, & O'Keefe, 1998), and topographic disorientation is produced by right-hemisphere, perisplenial lesions (Takahashi, Kawamura, Shiota, Kasahata, & Hirayama, 1997). In contrast, the ventral PCC (vPCC) evaluates the emotional and nonemotional contents of sensory objects and contexts in terms of self-relevance (Johnson et al., 2002; Phan, Wager, Taylor, & Liberzon, 2002), it is activated to a greater extent by familiar places than objects (Sugiura, Shah, Zilles, & Fink, 2005), and it receives input from the ventral visual stream (Vogt et al., 2006). The elegant study by Sugiura et al. showed that vPCC has particularly high activity during exposure to familiar places over objects and dPCC is most active during presentation of familiar objects. Coactivation of RSC along

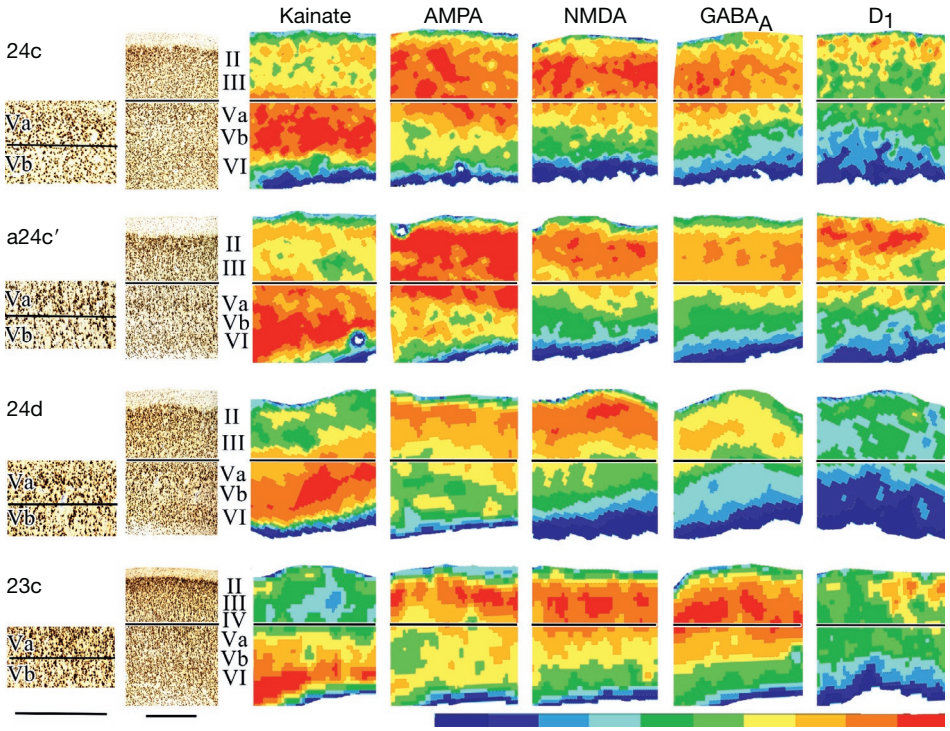

Figure 8 Sulcal area cytology with matched receptor binding from Palomero-Gallagher and Zilles (2009): area 24c in ACC, areas a24c′ and 24d in MCC, and area 23c in dPCC. The lines on each cytoarchitectural area mark the border between layers IIIc and Va, and on the left magnified sections, it is between layers Va and Vb. Of particular note is that layer Vb neurons are largest in areas a24c′ and 24d, kainate binding is highest in layer V of area 24c and progressively decreases in caudal areas, AMPA receptors are mainly in superficial layers and decrease caudally, and dopamine-1 receptors are at highest levels in area a24c′ and quite low in other areas. Scale bars, 500 μm; autoradiograph scale for relative comparisons.

with dPCC suggests that reciprocal connections among these regions (Vogt & Pandya, 1987) have important functional consequences. Thus, vPCC determines self-relevance via connections with sACC where long-term memories of valenced events are stored and RSC where self-referenced episodic memories are stored. Such coding is then directed to MCC for skeletomotor system output. In contrast, dPCC has a closer link with MCC and appears to be associated with sensorimotor orientation in space and rapid adjustments to visuospatial needs in the context of the dorsal multisensory stream (Vogt et al., 2006).

The PCC is composed of areas 23 and 31, and its two-part parcellation is based on primate cytology (Vogt Vogt, Farber, & Bush, 2005, 2006), monkey connections (Shibata & Yukie, 2003, 2009), human functional imaging (Vogt et al., 2006), and multireceptor binding (Palomero-Gallagher et al., 2009). The monkey vPCC was recognized by Goldman-Rakic, Selemon, and Schwartz (1984) as the caudomedial lobule (CML) with heavy frontal connections, and later, its intracingulate connections with sACC were reported (Vogt & Pandya, 1987). Further, Shibata and Yukie (2003) showed differential thalamic afferents with dPCC receiving unique inputs from the mediodorsal, central lateral, ventral anterior, and lateral nuclei. **Figure 9** compares a pair of sections dorsal to the splenium (b) and caudal to it (e). The latter location is the CML (**Figure 9(e)**), which is an extension of the posterior cingulate gyrus and is composed of ventral area 23 (Vogt et al., 2006). **Figure 9(b)** (NeuN) shows the indusium griseum (IG) and subicular rudiment (Sub) forming the fasciolar gyrus above the corpus callosum. Ectosplenial area 26 is the first part of the ventral bank of the CG, is transitional to area 29, and is composed mainly of an external pyramidal layer. Area d23b has less densely packed layer II neurons, smaller pyramids in layer IIIc, thin layer Va, and a relatively sparse layer Vb in comparison with v23b (**Figure 9(e)**; CML). Intermediate neurofilament proteins are expressed by large pyramids in layers III and Va and are more extensive in v23b than in d23b (Vogt et al., 2006). Also, SMI32-labeled pyramids in layer Va of area d23b are sparse in comparison with those in area v23b. Area 23c, in contrast, has a thin layer IV and a very dense layer Va, and layer IIIc is composed of larger neurons. The thickness of layers II–IV in area 23c is significantly greater than that of layers V–VI (layer Va marked with red asterisk in **Figure 9(b)** and layer III in **Figure 9(c)**). Finally, ventral area 31 (v31) (**Figure 9(e)**) has a more pronounced layer II, quite large layer IIIc pyramids, a broad layer IV, a thick layer Va, and a less dense layer Vb than area 23c. Area 31 has the thickest layer IV of any cingulate area.

RSC and the Perisplenial Location

Human imaging has been plagued by mislocalizing RSC due mainly to Talairach and Tournoux's (1988) interpretation of Brodmann's map. While the latter map implied that RSC is in the cas, the former authors extended areas 29 and 30 onto the gyral surface caudal to the splenium. We analyzed this issue in detail (Vogt Vogt, Perl, & Hof, 2001) and found no support for it. A number of studies report small 'retrosplenial' strokes (e.g., Takahashi et al., 1997) where the stroke not only is limited to

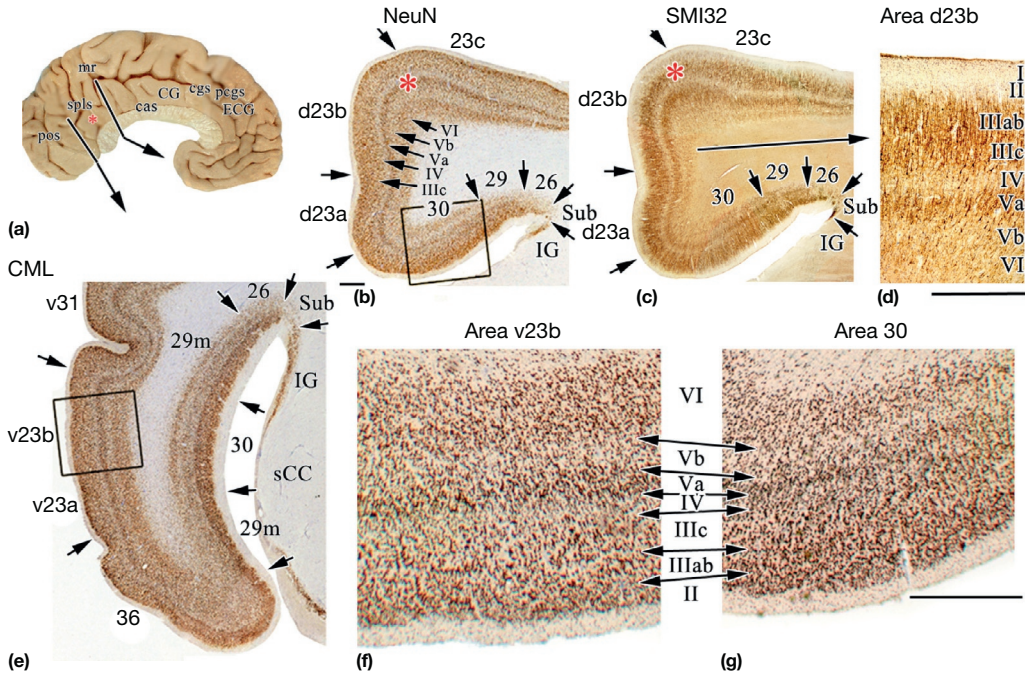

Figure 9 Histology of posterior cingulate and retrosplenial cortices. (a) Medial surface with section orientations. The asterisk marks a splenial sulcus (spls) branch that extends to the callosal sulcus (cas). (b) dPCC just caudal to dysgranular area 23d. The asterisk emphasizes the layer Va border between areas d23b and 23c, and the square is the position of area 30 enlargement in (g) and (c) matched SMI32 section to (b), with the border of layer III marked with an asterisk between areas d23b and 23c and an arrow showing area d23b enlarged in (d). (e) Caudomedial lobule (CML; NeuN) with a box for the cortex enlarged for (f) v23b. (f, g) show the cytoarchitecture of the surface cortex on the CML and area 30 in the callosal sulcus. The key point is that area 30 does not extend onto the caudal surface of the cingulate gyrus as shown in the Talairach and Tournoux (1988) atlas. Instead, areas 29 and 30 are buried in the caudal end of the cas around the splenium of the corpus callosum (sCC). CG, cingulate gyrus; cgs, cingulate sulcus; ECG, external cingulate gyrus; IG, indusium griseum; mr, marginal ramus of the cgs; pcgs, paracingulate sulcus; pos, parieto-occipital sulcus; Sub, dorsal subicular rudiment. All scale bars are 1 mm.

RSC but also involves area 23 and part of area 31; white matter damage assures that the resulting symptoms are not solely due to damage to areas 29 and 30. This literature also blurs the relationship between the retrosplenial location around the splenium and RSC defined cytoarchitecturally. To avoid this ongoing confusion, we suggest the term 'perisplenial' when referring to a general location around the splenium and reserving the word 'retrosplenial' for cytoarchitectonically defined areas 29 and 30. In the few instances where there is adequate spatial resolution to locate RSC (Sugiura et al., 2005), 'retrosplenial' is a valid term.

Area 30 (Figure 9(g)) has a wide layer II from which layer IIIab pyramids are poorly differentiated compared with that in area v23b. Layer IIIc is clearly present but layer IV is dysgranular; that is, it is variable in thickness and pyramids in layers IIIc and Va often intermingle. Layer Va is not as broad and neuron dense as layer VI in area v23b and is substantially more elaborated than in area 30. These many differences assert the claim that area 30 is not present on the caudal cingulate gyral surface. Area 30, however, is also located in the cas around the splenium (Figure 9(e), sCC) where it is flanked by area 29m.

Magnetic Resonance Imaging: Subregions and Connections

Although cytoarchitecturally defined areas and subregions should serve as the basis of functional and connection studies, there is an alternative approach. Torta and Cauda (2011) divided cingulate cortex into 12 equally spaced regions of interest (ROIs) for a meta-analytic coactivation analysis. The 12 ROIs were associated with different combinations of activity including reward, attention, pain discrimination, emotion, language, action execution, memory, semantic discrimination, and episodic recall. Findings such as the role of ROI 8/area d23 (dPCC) in motor functions including action execution and finger tapping are well known (Vogt & Sikes, 2009), and there was a lack of precision of imaging outcomes based on task design and vague definition of behavior and emotion that reflect reward-related or pain-related activations. Further, attention may underlie most of the tasks but is identified as a unique function in one part of cingulate cortex. Thus, conclusions from a study that explicitly overlooked anatomical organization did not expand understanding of cingulate functions, and this non-structure/function approach emphasizes the importance of beginning with the cytoarchitectural map rather than the opposite.

Diffusion Tensor Imaging Tractography

One of the best studies of human cingulate connections with MR diffusion tensor imaging (DTI) is that of Beckmann, Johansen-Berg, and Rushworth (2009). They determined cingulate connectivity with an algorithm to search for regional variations in the probabilistic connectivity profiles of all cingulate voxels with the rest of the brain; nine subregions

emerged. The probabilities of a connection between cingulate cortex and 11 predefined ROIs were also calculated, and cingulate voxels with a high probability of connection with the different targets formed separate clusters (Figure 10(a)). An explicit attempt was made to relate the connection clusters to cytoarchitectural entities, but note the following: Although #1 was in sACC, #2 is split between this subregion and pACC; although #3 is restricted to pACC, it does not differentiate areas 24 and 32; #4 is in aMCC and #6 in pMCC; however, #5 and #7 extend throughout MCC and #8/#9 engages the entire PCC. Thus, these clusters have some correlation with subregions but do not designate cytoarchitectural areas because cingulate connections do not respect cytoarchitectural borders.

Figure 11 shows five of the connections and findings for similar areas in the monkey. While it is not expected that human and monkey connections have an exact correspondence, there should be some broad similarities. The amygdala cluster is in sACC, and while the central nucleus of the amygdala does project to sACC (Chiba, Kayahara, & Nakano, 2001), the lateral and accessory basal nuclei have extensive projections throughout ACC and aMCC. Although the hippocampus has limited cingulate connections, parahippocampal cortex has robust, widely distributed, and reciprocal connections with most of the CG. Clusters 1, 2, and 7–9 reflect this fact to some extent, although monkey connections predict a very robust projection that should include all 9 clusters. The ventral stratum identified mainly sACC and a small extension to area 33 along the cas. Again, this appears to be but a part of a much larger projection for this region and the dorsal striatum. Finally, clusters 1–2 and 5–7 were associated with the parietal ROI, and this reflects to some extent the connection shown in monkeys. Thus, some critical connectivity in the human cingulate cortex has been identified. From the outset, however, we know that connections are not limited to single areas or subregions. Thus, cytoarchitecturally defined ROIs would be a better method for analyzing cingulate connectivity and functions. Indeed, Yu et al. (2011) evaluated the cingulate subregional model with resting-state functional connectivity and supported unique contributions of each subregion in different cortical networks.

Parcellation with Landmarks

Figure 11(b) shows the outcome of a study by Destrieux et al. (2010). They performed a computer-assisted hand parcellation to classify each vertex as sulcal or gyral and then subparcelled the cortex into 74 'labels' per hemisphere. Twelve datasets were used to develop rules and algorithms that produced labels consistent with anatomical rules and automated computational parcellation. This approach localized six cingulate ROIs; ROI 32 incorporated area 25 but not the remainder of sACC; six was in pACC, seven in aMCC, eight in pMCC, nine in

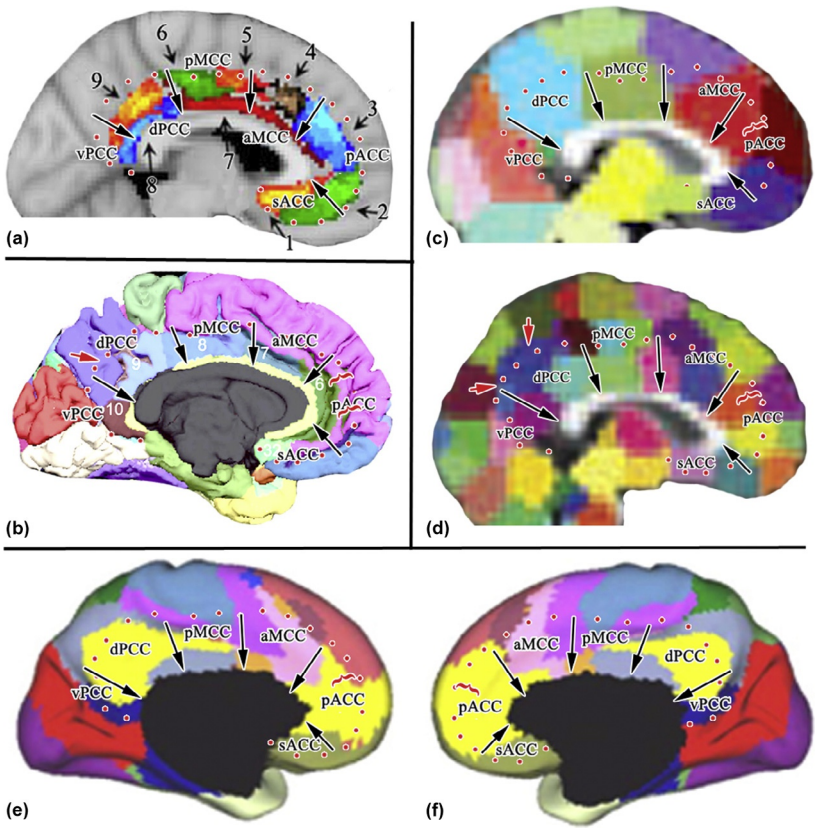

Figure 10 Medial surfaces from MRI studies. In all instances, the subregional borders are marked with arrows, and the external edge of the cingulate cortex is marked with red dots. Red arrows in (b) and (d) emphasize mismatches between the boundary of cingulate cortex and the maps, and red parentheses emphasize where area 32 should be located in the maps. (a) Beckmann et al. (2009), (b) Destrieux, Fischl, Dale, and Halgren (2010), (c, d) Craddock, James, Holtzheimer, Hu, and Mayberg (2012) for 50 and 1000 specified ROIs, respectively, (e) left and (f) right hemispheres from Yeo, Krienen, Sepulcre, et al. (2011).

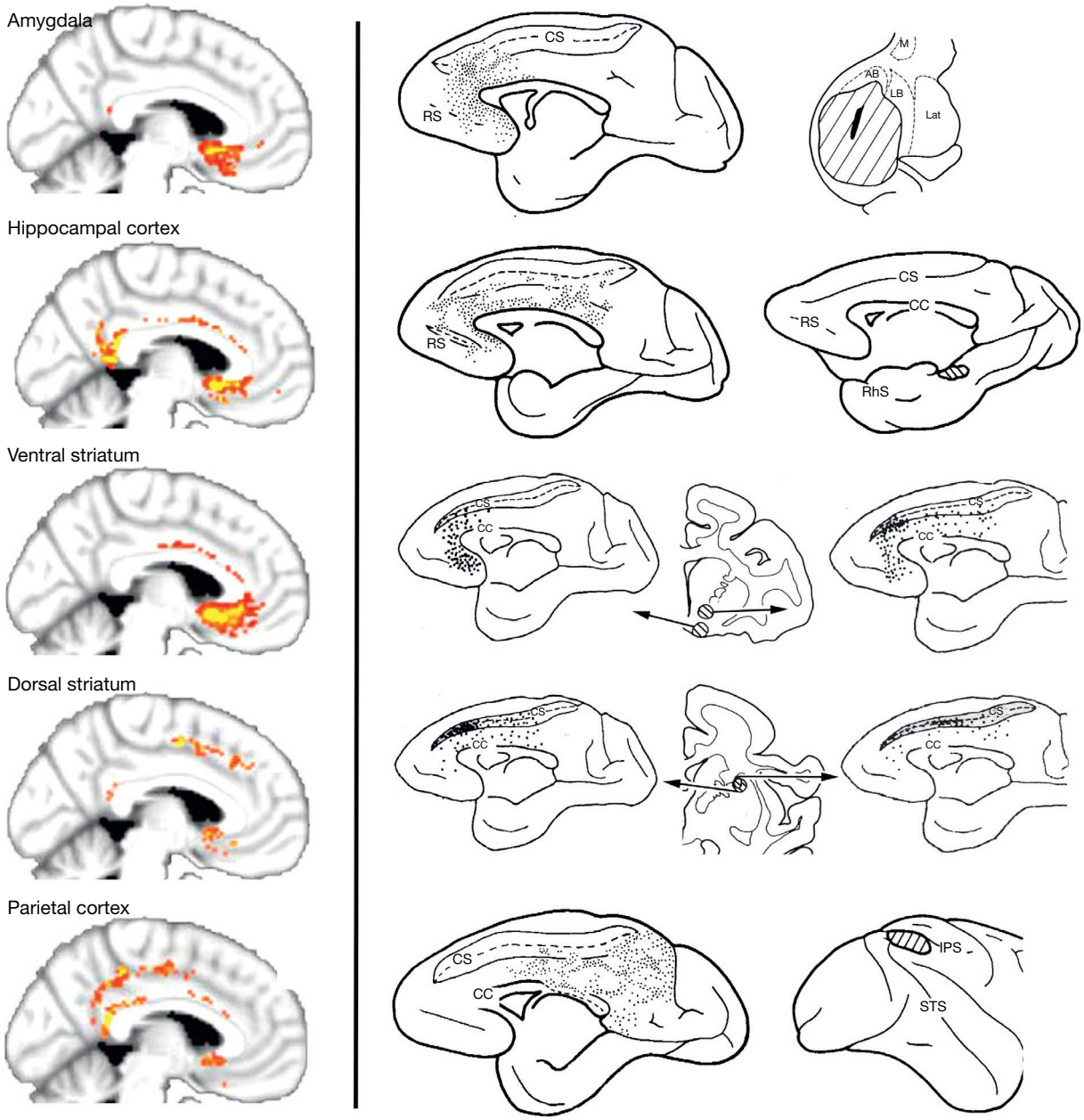

Figure 11 Comparison of human connections shown by Beckmann et al. (2009) and those for monkey; striatal monkey connections from Kunishio and Haber (1994) and all others from Vogt and Pandya (1987).

dPCC, and ten in vPCC. Area 32 on the ECG was not part of pACC or aMCC (red brackets), and part of dPCC was not included with ROI 9 (red arrow). Thus, this cingulate model is close in many ways to the cytoarchitectural observations and could be modified to accommodate these few shortcomings.

Local Connections

Craddock et al. (2012) used a data-driven method to generate an ROI atlas by parceling whole-brain resting-state functional MRI (fMRI) data into spatially coherent regions of homogeneous functional connectivity. ROI size and hence the number of ROIs in a parcellation had the greatest impact on their suitability for functional connectivity analysis. Figure 11 shows the outcome of specifying either 50 (c) or 1000 (d) ROIs. There is some correspondence in the 50 ROI map to the six cingulate subregions in the rostrocaudal (y-axis) plane, but there is no relationship to areas in the dorsoventral (z-axis) as the ROIs clearly extend beyond cingulate cortex and do not identify area 32 of the ECG. These investigators state that parcellation results containing higher numbers of ROIs (e.g., 1000) most accurately represent functional connectivity patterns at the voxel scale and are preferable when interpretability can be sacrificed for accuracy. Although ROIs in the cingulate cortex reflect some cytoarchitectural boundaries, they still do not identify area 32 of the ECG (red parenthesis) nor are they

accurate in the dorsal part of dPCC (red arrows). Thus, this method identifies some relationships with boundaries set by cytoarchitectural analyses; however, they are not exact and may be viewed as confirmation of cytoarchitectural studies to the extent that there are functional connectivity patterns supporting the rostrocaudal distribution of subregions.

Network Connections

Yeo et al. (2011) published a study of resting-state functional connectivity using surface-based alignment, and **Figure 11(e)** and **11(f)** shows their results. The most striking correspondences of these connections with the cytoarchitectural map are in sACC, pACC, and dPCC, which were uniquely identified, and the differentiation of aMCC and pMCC. Sites of discordance include the failure to identify area 32, the premotor areas in aMCC, RSC is combined with PCC and heterogeneity in vPCC. Of course, these are functional networks that do not necessarily require concordance with cytoarchitectural observations, although it is a concern that area 32 does not stand out as having unique connectivities.

Yu et al. (2011) evaluated resting-state functional connectivity of each cingulate subregion from a network perspective; each subregion was integrated in predescribed functional networks and showed anticorrelated resting-state fluctuations. The sACC and pACC were involved in an affective network and anticorrelated with the sensorimotor and cognitive networks, while the pACC also correlated with the default-mode network and anticorrelated with the visual network. The aMCC was correlated with the cognitive and sensorimotor networks and anticorrelated with the visual, affective, and default-mode networks, whereas the pMCC correlated with the sensorimotor network and anticorrelated with the cognitive and visual networks. The dPCC and vPCC involved in the default-mode network and anticorrelated with the sensorimotor, cognitive, and visual networks, and RSC was mainly correlated with the PCC and thalamus. Based on this hypothesis-driven approach, they confirmed the subregional analysis in terms of functional neuroanatomy.

Correlations as Connections and Neuropathology

The premise of basal glucose metabolism or resting fMRI correlations is that regions with similar levels of activity at rest are more likely to discharge together and engage in common information transfers than regions with substantially different levels of resting activity. Also, if direct connections have been demonstrated between a pair of areas in the monkey, there is a high probability that such sharing will occur. For example, seeding of basal glucose metabolism was used to evaluate correlations of dPCC and vPCC to determine circuits that differentiate these two subregions identified anatomically (Vogt et al., 2006). A major problem identifying connections arises when they are assessed in disease states. When new 'connections' are found with seeding/correlation studies, does this mean that there has been sprouting to form a new monosynaptic connection or has the disease itself altered metabolism and blood flow in a way that generates a new correlation when a new connection has not grown?

Mainero, Boshyan, and Hadjikhani (2011) used resting-state fMRI to compare the functional connectivity between the periaqueductal gray (PAG) and areas involved in nociception and somatic sensation in subjects with migraine and healthy controls when the former were pain-free (**Figure 12(c)**). They showed stronger 'connectivity' between the PAG and nociceptive and somatosensory areas in migraineurs. From a medial surface perspective, however, it appears that pACC and aMCC have a similar level of PAG correlations. Also, there are extensive correlations in PCC and parietal and visual cortices that have little or nothing to do with pain (**Figure 12**(c2)).

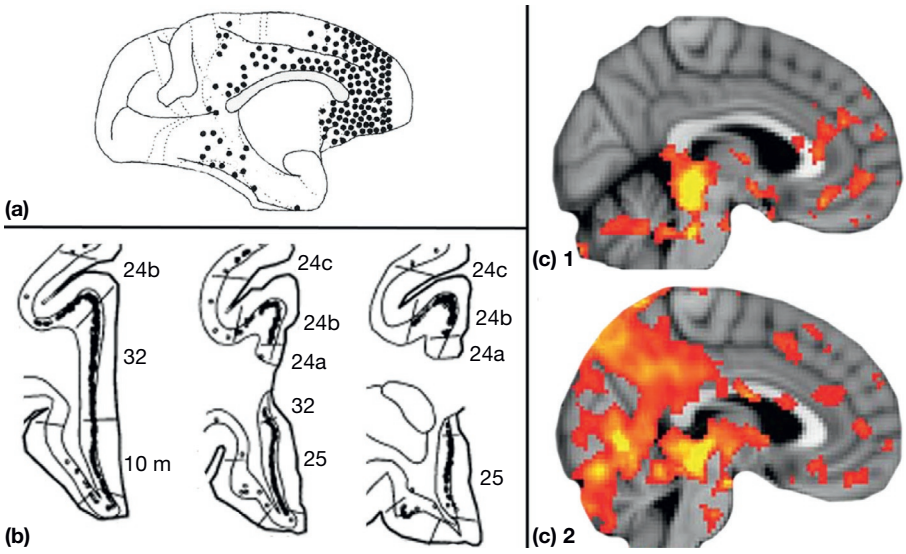

Figure 12 (a) Topographic projections to the periaqueductal gray (Dujardin & Jürgens, 2005; labeled neurons observed in all cases). Distribution of PAG projection neurons in layer V of ACC (An, Bandler, Öngür, & Price, 1998). (c1) Correlations of fMRI voxels with PAG resting state in healthy controls and (c2) PAG correlations in migraineurs (Mainero et al., 2011). The vast majority of PAG correlations in the migraine state do not represent PAG connections.

Moreover, the PAG only receives rostral cortical afferents, which are not reciprocal. Figure 12 shows cortical PAG afferents topographically (a) and by their layer of origin (b) in the monkey. The following points are of note: (a) although PCC has limited projections to the PAG, no correlations are in the control cases; (b) projections from ACC and aMCC are massive, while the correlations are weak in the rostral part of aMCC and nonexistent caudally; (c) correlations observed in the migraineurs in PCC and parietal and visual cortices do not represent connections. It appears that bouts of cortical spreading depression experienced during migraine have altered blood flow that reflects basal levels normally seen in the PAG; however, the correlations likely do not represent connections.

In conclusion, although the connectivity study of Yu et al. (2011) confirmed unique interactions of cingulate subregions with predetermined networks, DTI tractography shows only weak connectivity of cingulate cortex. Since afferents never terminate in a single area and efferents to a particular site do not arise from single areas, strict correlations between cytology and connections cannot be expected. Indeed, area 32′ is one of the more interesting areas from a functional perspective in its role in feedback-mediated decision making (Bush, 2009), yet none of the connection studies identifies area 32′ as a unique area. Also, low-density projections are not observed (e.g., amygdala projections to PCC; Buckwalter, Schumann, & Van Hoesen, 2008), and cingulate sulci cannot be used to guide locating areas. Where connections are particularly dense and concentrated, like those between the mammillary bodies and anterior thalamic nuclei, DTI provides a more compelling picture of connectivity; however, such studies provide limited information when applied to cingulate cortex itself (Granzieraa et al., 2011).

The cingulate subregional model based on cytoarchitecture and receptor binding evolved in tandem with functional imaging to produce a relatively coherent perspective on cingulate organization. The purpose of the subregional model, however, is not to simply provide labels and a descriptive framework, but to understand structure/function units and a context for predicting the role of cingulate subregions in complex cortical networks.

See also: **INTRODUCTION TO ANATOMY AND PHYSIOLOGY**: Cytoarchitectonics, Receptorarchitectonics, and Network Topology of Language; Cytoarchitecture and Maps of the Human Cerebral Cortex; Functional Connectivity; Quantitative Data and Scaling Rules of the Cerebral Cortex; Sulci as Landmarks; Von Economo Neurons; **INTRODUCTION TO CLINICAL BRAIN MAPPING**: Depression; Emotion and Stress; Pain Syndromes; **INTRODUCTION TO COGNITIVE NEUROSCIENCE**: Interactions between Attention and Emotion; Value Representation; **INTRODUCTION TO METHODS AND MODELING**: Diffusion Tensor Imaging; Tract Clustering, Labeling, and Quantitative Analysis; **INTRODUCTION TO SOCIAL COGNITIVE NEUROSCIENCE**: Emotion Perception and Elicitation; Emotion Regulation; Empathy; How the Brain Feels the Hurt of Heartbreak: Examining the Neurobiological Overlap Between Social and Physical Pain; Mentalizing; **INTRODUCTION TO SYSTEMS**: Cortical Action Representations; Emotion; Hubs and Pathways; Large-Scale Functional Brain Organization; Neural Networks Underlying Novelty Processing; Pain: Acute and Chronic; Reward.

References

Amunts, K., Malikovic, A., Mohlberg, H., Schormann, T., & Zilles, K. (2000). Brodmann's areas 17 and 18 brought into stereotaxic space – Where and how variable? *NeuroImage*, *11*, 66–84.

An, X., Bandler, R., Öngür, D., & Price, J. L. (1998). Prefrontal cortical projections to longitudinal columns in the midbrain periaqueductal gray in macaque monkeys. *Journal of Comparative Neurology*, *401*, 455–479.

Bancaud, J., & Talairach, J. (1992). Clinical semiology of frontal lobe seizures. *Advances in Neurology*, *57*, 3–58.

Beckmann, M., Johansen-Berg, H., & Rushworth, M. F. S. (2009). Connectivity-based parcellation of human cingulate cortex and its relation to functional specialization. *Journal of Neuroscience*, *29*, 1175–1190.

Berthoz, A. (1997). Parietal and hippocampal contribution to topokinetic and topographic memory. *Philosophical Transactions of the Royal Society, B: Biological Sciences*, *352*, 1437–1448.

Biber, M. P., Kneisley, L. W., & LaVail, J. H. (1978). Cortical neurons projecting to the cervical and lumbar enlargements of the spinal cord in young and adult rhesus monkeys. *Experimental Neurology*, *59*, 492–508.

Braak, H. (1976). A primitive gigantopyramidal field buried in the depth of the cingulate sulcus of the human brain. *Brain Research*, *109*, 219–233.

Brodmann, K. (1909). *Vergleichende lokalisationslehre der grosshirnrinde in ihren prinzipien dargestellt auf grund des zellenbaues*. Leipzig: Barth.

Buckwalter, J. A., Schumann, C. M., & Van Hoesen, G. W. (2008). Evidence for direct projections from the basal nucleus of the amygdala to retrosplenial cortex in the Macaque monkey. *Experimental Brain Research*, *186*, 47–57.

Bush, G. (2009). Dorsal anterior midcingulate cortex: Roles in normal cognition and disruption in attention-deficit/hyperactivity disorder. In B. A. Vogt (Ed.), *Cingulate neurobiology and disease* (pp. 245–274). London: Oxford University Press.

Bush, G., Luu, P., & Posner, M. I. (2000). Cognitive and emotional influences in anterior cingulate cortex. *Trends in Cognitive Sciences*, *4*, 215–222.

Cajal, R. Y. (1999). *Advice for a young investigator*. Cambridge, MA: MIT Press, translated by Swanson, N. and Swanson, L. W.

Chiba, T., Kayahara, T., & Nakano, K. (2001). Efferent projections of infralimbic and prelimbic areas of the medial prefrontal cortex in the Japanese monkey, *Macaca fuscata*. *Brain Research*, *888*, 83–101.

Craddock, R. C., James, G. A., Holtzheimer, P. E., III, Hu, X. P., & Mayberg, H. S. (2012). A whole brain fMRI atlas generated via spatially constrained spectral clustering. *Human Brain Mapping*, *33*, 1914–1928.

Destrieux, C., Fischl, B., Dale, A., & Halgren, E. (2010). Automatic parcellation of human cortical gyri and sulci using standard anatomical nomenclature. *NeuroImage*, *53*, 1–15. http://dx.doi.org/10.1016/j.neuroimage.2010.06.010.

Dujardin, E., & Jürgens, U. (2005). Afferents of vocalization-controlling periaqueductal regions in the squirrel monkey. *Brain Research*, *1034*, 114–131.

Enriquez-Geppert, S., Eichele, T., Specht, K., Kugel, H., Pantev, C., & Huster, R. J. (2013). Functional parcellation of the inferior frontal and midcingulate cortices in a Flanker-stop-change paradigm. *Human Brain Mapping*, *34*(7), 1501–1514.

Escobedo, F., Fernández-Guardiola, A., & Solis, G. (1973). Chronic stimulation of the cingulum in humans with behavior disorders. In L.V. Laitinen & K. E. Livingston (Eds.), *Surgical approaches in psychiatry* (pp. 65–68). Lancaster (UK), Baltimore: MTP.

George, M. S., Ketter, T. A., Gill, D. S., Haxby, J., Ungerleider, L. G., Herscovitch, P., et al. (1993). Brain regions involved in recognizing facial emotion or identity: An oxygen-15 PET study. *Journal of Neuropsychiatry and Clinical Neurosciences*, *5*, 384–394.

George, M. S., Ketter, T. A., Parekh, P. I., Horwitz, B., Herscovitch, P., & Post, R. M. (1995). Brain activity during transient sadness and happiness in healthy women. *The American Journal of Psychiatry*, *152*, 341–351.

Ghaem, O., Mellet, E., Crivello, F., Tzourio, N., Mazoyer, B., Berthoz, A., et al. (1997). Mental navigation along memorized routes activates the hippocampus, precuneus, and insula. *NeuroReport*, *8*, 739–744.

Goldman-Rakic, P. S., Selemon, L. D., & Schwartz, M. L. (1984). Dual pathways connecting the dorsolateral prefrontal cortex with the hippocampal formation and parahippocampal cortex in the rhesus monkey. *Neuroscience*, *12*, 719–743.

Grachev, I. D., Berdichevsky, D., Rauch, S. L., Heckers, S., Kennedy, D. N., Caviness, V. S., et al. (1999). A method for assessing the accuracy of intersubject registration of the human brain using anatomic landmarks. *NeuroImage*, *9*, 250–268.

Granzieraa, C., Hadjikhanif, N., Arzyc, S., Seeckd, M., Meulib, R., & Kruegere, G. (2011). In-vivo magnetic resonance imaging of the structural core of the Papez circuit in humans. *NeuroReport*, *22*, 227–231.

Habas, C. (2010). Functional connectivity of the human rostral and caudal cingulate motor areas in the brain resting state at 3 T. *Neuroradiology*, *52*, 47–59.
James, W. (1884). What is emotion? *Mind*, *9*, 188–205.
Johnson, S. C., Baxter, L. C., Wilder, L. S., Pipe, J. G., Heiserman, J. E., & Prigatano, G. P. (2002). Neural correlates of self-reflection. *Brain*, *125*, 1808–1814.
Kirsch, P., Schienle, A., Stark, R., Sammer, G., Blecker, C., Walter, B., et al. (2003). Anticipation of reward in a nonaversive differential conditioning paradigm and the brain reward system: An event-related fMRI study. *NeuroImage*, *20*, 1086–1095.
Kunishio, K., & Haber, S. N. (1994). Primate cingulostriatal projection: Limbic striatal versus sensorimotor striatal input. *Journal of Comparative Neurology*, *350*, 337–356.
Kwan, C. L., Crawley, A. P., Mikulis, D. J., & Davis, K. D. (2000). An fMRI study of the anterior cingulate cortex and surrounding medial wall activations evoked by noxious cutaneous heat and cold stimuli. *Pain*, *85*, 359–374.
Li, D. F., Freeman, A. W., Tran-Dinh, H., & Morris, J. G. (2003). A Cartesian coordinate system for human cerebral cortex. *Journal of Neuroscience Methods*, *125*, 137–145.
Luppino, G., Matelli, M., Camarda, R. M., Gallese, V., & Rizzolatti, G. (1991). Multiple representations of body movements in mesial area 6 and the adjacent cingulate cortex: An intracortical microstimulation study in the macaque monkey. *Journal of Comparative Neurology*, *311*, 463–482.
Maguire, E. A., Frith, C. D., Burgiss, N., Donnett, J. G., & O'Keefe, J. (1998). Knowing where things are: Parahippocampal involvement in encoding object locations in virtual large-scale space. *Journal of Cognitive Neuroscience*, *10*, 61–76.
Mainero, C., Boshyan, J., & Hadjikhani, N. (2011). Altered functional magnetic resonance imaging resting-state connectivity in periaqueductal gray networks in migraine. *Annals of Neurology*, *70*, 838–845.
Mayberg, H. S., Liotti, M., Brannan, S. K., McGinnis, S., Mahurin, R. K., Jerabek, P. A., et al. (1999). Reciprocal limbic-cortical function and negative mood: Converging PET findings in depression and normal sadness. *The American Journal of Psychiatry*, *156*, 675–682.
Meyer, G., McElhaney, M., Martin, W., & McGraw, C. P. (1973). Stereotactic cingulotomy with results of acute stimulation and serial psychological testing. In L. V. Laitinen & K. E. Livingston (Eds.), *Surgical approaches in psychiatry* (pp. 39–58). Lancaster (UK), Baltimore: MTP.
Murtha, S., Chertkow, H., Beauregard, M., Dixon, R., & Evans, A. (1996). Anticipation causes increased blood flow to the anterior cingulate cortex. *Human Brain Mapping*, *4*, 103–112.
Nowinski, W. L. (2001). Modified Talairach landmarks. *Acta Neurochirurgica*, *143*, 1045–1057.
Nudo, R. J., & Masterton, R. B. (1990). Descending pathways to the spinal cord, III: Sites of origin of the corticospinal tract. *Journal of Comparative Neurology*, *296*, 559–583.
Olson, C. R., Musil, S. Y., & Goldberg, M. E. (1993). Posterior cingulate cortex and visuospatial cognition: Properties of single neurons in the behaving monkey. In B. A. Vogt & M. Gabriel (Eds.), *Neurobiology of cingulate cortex and limbic thalamus*. Boston: Birkhäuser.
Olson, C. R., Musil, S. Y., & Goldberg, M. E. (1996). Single neurons in posterior cingulate cortex of behaving macaque: Eye movement signals. *Journal of Neurophysiology*, *76*, 3285–3300.
Palomero-Gallagher, N., Mohlberg, H., Zilles, K., & Vogt, B. A. (2008). Cytology and receptor architecture of human anterior cingulate cortex. *Journal of Comparative Neurology*, *508*, 906–926.
Palomero-Gallagher, N., Schleicher, A., Zilles, K., & Vogt, B. A. (2013). Differentiation of monkey area 32 and human comparative analysis. *Journal of Comparative Neurology*, *521*, 3272–3286.
Palomero-Gallagher, N., Vogt, B. A., Mayberg, H. S., Schleicher, A., & Zilles, K. (2009). Receptor architecture of human cingulate cortex: Evaluation of the four region neurobiological model. *Human Brain Mapping*, *30*, 2336–2355.
Palomero-Gallagher, N., & Zilles, K. (2009). Transmitter receptor systems in cingulate regions and areas. In B. A. Vogt (Ed.), *Cingulate neurobiology and disease* (pp. 31–63). London: Oxford University Press.
Phan, K. L., Wager, T., Taylor, S. F., & Liberzon, I. (2002). Functional neuroanatomy of emotion: A meta-analysis of emotion activation studies in PET and fMRI. *NeuroImage*, *16*, 331–348.
Pool, J. L. (1954). The visceral brain of man. *Journal of Neurosurgery*, *11*, 45–63.
Pool, J. L., & Ransohoff, J. (1949). Autonomic effects on stimulating rostral portion of cingulate gyri in man. *Journal of Neurophysiology*, *12*, 385–392.
Posner, M. I., Peterson, S. E., Fox, P. T., & Raichle, M. E. (1988). Localization of cognitive operations in the human brain. *Science*, *240*, 1627–1631.
Shibata, H., & Yukie, M. (2003). Differential thalamic connections of the posteroventral and dorsal posterior cingulate gyrus in the monkey. *European Journal of Neuroscience*, *18*, 1615–1626.
Shibata, H., & Yukie, M. (2009). Temporocingulate interactions in the monkey. In B. A. Vogt (Ed.), *Cingulate neurobiology and disease* (pp. 145–162). London: Oxford University Press.
Shima, K., Aya, K., Mushiake, H., Inase, M., Aizawa, H., & Tanji, J. (1991). Two movement-related foci in the primate cingulate cortex observed in signal-triggered and self-paced forelimb movements. *Journal of Neurophysiology*, *65*, 188–202.
Shima, K., & Tanji, J. (1998). Role for cingulate motor area cells in voluntary movement selection based on reward. *Science*, *282*, 1335–1338.
Shin, L. M., Lasko, N. B., Macklin, M. L., Karpf, R. D., Milad, M. R., Orr, S. P., et al. (2009). Resting metabolic activity in the cingulate cortex and vulnerability to posttraumatic stress disorder. *Archives of General Psychiatry*, *66*, 1099–1107.
Sugiura, M., Shah, N. J., Zilles, K., & Fink, G. R. (2005). Cortical representations of personally familiar objects and places: Functional organization of the human posterior cingulate cortex. *Journal of Cognitive Neuroscience*, *17*, 1–16.
Takahashi, N., Kawamura, M., Shiota, J., Kasahata, N., & Hirayama, K. (1997). Pure topographic disorientation due to right retrosplenial lesion. *Neurology*, *49*, 464–469.
Talairach, J., Bancaud, J., Geier, S., Bordas-Ferrer, M., Bonis, A., & Szikla, G. (1973). The cingulate gyrus and human behavior. *Electroencephalography and Clinical Neurophysiology*, *34*, 45–52.
Talairach, J., & Tournoux, P. (1988). *Co-planar stereotaxic atlas of the human brain*. Stuttgart and New York: Georg Thieme.
Torta, D. M., & Cauda, F. (2011). Different functions in the cingulate cortex, a meta-analytic connectivity modeling study. *NeuroImage*, *56*, 2157–2172.
Vogt, B. A. (2009a). Regions and subregions of the cingulate cortex. In B. A. Vogt (Ed.), *Cingulate neurobiology and disease* (pp. 3–30). London: Oxford University Press.
Vogt, B. A. (2009b). Architecture, neurocytology and comparative organization of monkey and human cingulate cortices. In B. A. Vogt (Ed.), *Cingulate neurobiology and disease* (pp. 65–93). London: Oxford University Press.
Vogt, B. A., & Palomero-Gallagher, N. (2012). Cingulate cortex. In G. Paxinos & J. K. Mai (Eds.), *The human nervous system* (pp. 943–987) (3rd ed.). Amsterdam: Academic Press (Chapter 25).
Vogt, B. A., & Pandya, D. N. (1987). Cingulate cortex of rhesus monkey. *II. Cortical afferents*. *Journal of Comparative Neurology*, *262*, 271–289.
Vogt, B. A., & Paxinos, G. (2014). Cytoarchitecture of mouse and rat cingulate cortex with human homologies. *Brain Structure and Function*, *219*, 185–192. http://dx.doi.org/10.1007/s00429-012-0493-3.
Vogt, B. A., & Sikes, R. W. (2009). Cingulate nociceptive circuitry and roles in pain processing: The cingulate premotor pain model. In B. A. Vogt (Ed.), *Cingulate neurobiology and disease* (pp. 312–338). London: Oxford University Press.
Vogt, C., & Vogt's, O. (1919). Allegemeine ergebnisse unserer hirnforschung. *Journal für Psychologie und Neurologie*, *25*, 279–462.
Vogt, B. A., & Vogt, L. J. (2009). Opioids, placebos and descending control of pain and stress systems. In B. A. Vogt (Ed.), *Cingulate neurobiology and disease* (pp. 339–364). London: Oxford University Press.
Vogt, B. A., Berger, G. R., & Derbyshire, S. W. J. (2003). Structural and functional dichotomy of human midcingulate cortex. *European Journal of Neuroscience*, *18*, 3134–3144.
Vogt, B. A., Vogt, L. J., & Laureys, S. (2006). Cytology and functionally correlated circuits of posterior cingulate areas. *NeuroImage*, *29*, 452–466.
Vogt, B. A., Nimchinsky, E. A., Vogt, L. J., & Hof, P. R. (1995). Human cingulate cortex: Surface features, flat maps, and cytoarchitecture. *Journal of Comparative Neurology*, *359*, 490–506.
Vogt, B. A., Vogt, L., Farber, N. B., & Bush, G. (2005). Architecture and neurocytology of the monkey cingulate gyrus. *Journal of Comparative Neurology*, *485*, 218–239.
Vogt, B. A., Vogt, L. J., Perl, D. P., & Hof, P. R. (2001). Cytology of human caudomedial cingulate, retrosplenial, and caudal parahippocampal cortices. *Journal of Comparative Neurology*, *438*, 353–376.
Yeo, B. T.T, Krienen, F. M., Sepulcre, J., Sabuncu, M. R., Lashkari, D., Hollinshead, M., et al. (2011). The organization of the human cerebral cortex estimated by intrinsic functional connectivity. *Journal of Neurophysiology*, *106*, 1125–1165.
Yu, C., Zhou, Y., Liu, Y., Jiang, T., Dong, H., Zhang, Y., et al. (2011). Functional segregation of the human cingulate cortex is confirmed by functional connectivity based neuroanatomical parcellation. *NeuroImage*, *54*, 2571–2581.